Statistical Analysis of Banded Periodic Patterns in Arid Grasslands

A THESIS

Presented to
The Faculty of the Department of Environmental Sciences of
Colorado College

In Partial Fulfillment of the Requirements for the Degree
Bachelor of Arts

By
Sophie Nasvik

February 2021

Abstract

As a result of climate change driving global resource scarcity, ecosystems are pressured to respond to recent regime shifts. Specifically, in arid ecosystems, stronger droughts and rapidly rising annual temperatures are increasing water scarcity and forcing arid landscapes to become more resilient to these environmental changes. Self-organized patchiness of vegetation structure has been observed in arid ecosystems worldwide as a response to water scarcity. Mathematical models have explored the significance of these patterned landscapes and have suggested their existence as a sign of resiliency in arid ecosystems, but also as a possible forewarning of a catastrophic shift to a homogenous bare ecosystem. Several factors, like slope orientation and mechanisms such as positive feedbacks and bistability, create a periodic banded vegetation pattern. We investigated the formation of the periodic banded vegetation patterns in Southern Colorado at Chico Basin Ranch. We expected the landscape at Chico Basin Ranch to start as a spatially random, homogenous landscape that developed periodic patterns over time in response to a change in climate. A Fast Fourier Transform (FFT) analysis method was developed on R Studio and then applied to high resolution imagery of the 1x2 km area of interest for the years 1999, 2003, 2015, 2017 and 2019. The quantitative analysis searched for statistically significant banded vegetation patterns, the dominant waves in each AOI and the orientation of the pattern. Climate trends observed in El Paso County, CO show an upward linear trend in temperature maxima/minima combined with three significant droughts which occurred during the 20-year period of this study. We observed a notable increase in significant banded vegetation patterns after the droughts occurred. We found that there are statistically significant banded vegetation patterns at Chico Basin Ranch and the coverage of significant patterns has increased since 1999 from 14.7% to 36% in 2019 of the AOI. The landscape at Chico Basin did not begin as a

spatially random homogenous landscape, as we had originally expected, but rather as a landscape with a low proportion of statistically significant patterns that was not spatially random. Generally, the patterns are oriented at ~90° (North). The effects of climate change could be driving the continued formation of the vegetation patterns at Chico Basin Ranch.

Introduction

Self-organized patchiness of vegetation structure in desert and arid ecosystems have been observed around the globe but have been studied in detail in arid regions of Africa and Australia (Dunkerley et. al, 2018). Arid ecosystems are defined as ecosystems with mean annual precipitation rates of 150-250 mm of rainfall during the growing season and 60 – 100 mm the rest of the year (Noy-Meir, 1973). Since rainfall is infrequent and variable throughout the year, competition for water is a necessary controlling factor that drives important processes in arid ecosystems (Noy-Meir, 1973).

This study will focus on the formation of a periodic anisotropic pattern that is dependent on slope characteristics and water availability. The patterns follow slope contour lines and improve water efficiency in arid ecosystems where water conservation is necessary (Valentin and d'Herbés, 1999; D'Odorico et. al, 2006). These patterns vary in length and width, alternating between bands of vegetated and bare sections (Figure 2).

Limited water resources in these regions force ecosystems to create efficient capture and storage mechanisms. The organization of vegetation bands on a downhill slope hinder surface runoff and promote more efficient water conservation. Spatial patterns are created under certain drought conditions (Vega and Montaña, 2011). The bare patches, called intergroves, create a smooth runoff surface for sheet flow the vegetated groves can absorb (Noy-Meir, 1973; Ludwig

et. al, 1998). It is a source (intergrove) to sink (grove) system (Valentin and d'Hérbes, 1999). Banded vegetation patterns are slope dependent and will not form on flat ground, as they play a necessary role in water collection from runoff (Dunkerley, 1999; Rietkerk et. al 2002; Dagbovie and Sherratt, 2014).

The differences in the soil profile of the groves and intergroves drive water infiltration during rainfall. The organization of vegetation bands on a downhill slope is aided by the different soil properties of the grove/intergrove bands. Intergrove sections promote runoff with smooth, crusted surface layers of soil that create a strong, stable soil surface which rainfall will not absorb easily into. The soil properties of the groves show a stark difference; the vegetation patches promote water absorption and retention (Dunkerley et. al 1999). This is due to the presence of roots and lower evaporation rates which are attributed to the reduction of radiation and wind speeds with vegetation cover (Noy-Meir, 1973).

General theory for the formation of periodic spatial patterns was originally developed by Turing in 1954 as a system of two interacting and diffusing agents: activator and inhibitor (Turing, 1953). This theory was later modified into a conceptual model of long-range inhibition and short-range facilitation. At a short range, there is a strong positive feedback loop between vegetation growth and soil moisture (Reitkerk et.al, 2004; D'Odorico et. al, 2005). Meaning, higher vegetation density will have a greater infiltration rate, and if there is enough water, root depth will increase which then increases infiltration and soil moisture, making the vegetation patches retain more water and continue to grow. At a larger scale, moisture in soil is depleted by vegetated patches. This depletion of moisture constitutes long-range inhibition, because the vegetation patches deplete water beyond their margins to levels that cannot sustain vegetation growth. There are several mechanisms for this long-range water depletion. Vegetation can

deplete runoff through higher infiltration, as mentioned previously. Vegetation can also deplete water through extensive root systems or via soil hydraulic conductivity, where soil water moves from areas of less negative water potential to that of more negative soil water potential (caused by local depletion of water resources by the roots) (Vandervaere et al, 1997).

Quantitative models have explored the formation of periodic banded vegetation patterns as a forewarning for a sudden catastrophic change (Reitkerk et. al, 2004). Multiple possible stable states and the sudden catastrophic shifts between them are typically a result of underlying positive feedbacks (Sheffer et. al, 2001; Sheffer and Carpenter, 2003); therefore, the facilitation that increases the ecological efficiency and resiliency can also extend the existence of the system into the assertion of external variables, such as rainfall, that do not allow for the establishment of the vegetation. This creates two equally plausible alternative states: grassland and desert. Bistability is often associated with sudden catastrophic shifts from one state to another that are hard to reverse. Several numerical models have explored the possibility that a decline in rainfall and the availability of water may lead to a sudden catastrophic shift in the environment. Instead of having two bistable states, plant cover declines rapidly and the ecosystem shifts to a homogenous bare environment. This bare state is stable and difficult to manipulate back into a vegetated ecosystem (Reitkerk et. al, 2004). It takes a major increase in the limiting resource—rainfall—to disturb the bare ecosystem enough to disrupt the stable state and renew vegetation cover (D'Odorico et. al, 2005). Before the catastrophic shift, two alternative stable states, the bare and the vegetated states, exist in these arid ecosystems. Bistability and positive feedback loops, as mentioned previously, are two factors that are seen to be the principles causing catastrophic ecosystem shifts (Reitkerk et. al, 2004; Sheffer and Carpenter, 2003). Studies link

the self-organized vegetation bands to catastrophic shifts, the emergence of the latent desertified equilibrium in the models coincides with the emergence of banded vegetation patterns.

It is important to note that the link between the catastrophic bifurcation and spatial patterning is still poorly understood. Quantitative mathematical models leave out several potentially important details including the rate and variability of precipitation and key details of plant life, history and physiology (Dunkerley et. al, 2018). Models also made the conclusion that if annual rainfall decreased at a rate that was slower, representing gradual climate change, stable vegetation bands would develop in order to accommodate this change in water availability (Chen et. al, 2015). Other studies have supported the hypothesis that vegetation patterns increase the efficiency and resiliency of arid ecosystems (D'Odorico et. al, 2006, 2005; Dunkerley et. al, 2018). A study by D'Odorico et. al (2006) interpreted the formation of patterns as a sign that dryland ecosystems were improving their productivity and chance for survival. The numerical models are an important aspect of the studies on vegetation patterns, and their findings need to be accounted for and recognized, however, should be thought of as an exploration and not a definitive conclusion. Numerical models serve as an exploration of these vegetation patterns. They are groundwork towards understand how specific spatial patterns might form and what they could mean. Quantitative models are an important part of gathering a better understanding of the mechanisms and dynamics of arid ecosystems, but they do not serve as a firm explanation to the formation and meaning of banded vegetation patterns. It is important to consider their findings moving forward, but these models must be paired local studies.

There are a wide diversity of locations and unique arid ecosystems that banded vegetation patterns have developed in. Local studies where the findings are more site-specific and include unique soil types, vegetation floristics, accurate mean annual rainfall, and rooting depths will

greatly increase the knowledge and understanding of dryland mechanisms and dynamics (Dunkerly et. al, 2018). These studies can pair direct observations with the outcomes of modelled predictions to compare the important similarities and differences between the two in order to make conclusions on if these vegetated bands are actually a forewarning for a catastrophic shift. As Bokulich (2014) explains, this will shift the research on vegetation bands from a "how possibly" explanation to a "how-actually" explanation.

Presently, there are not any studies where a catastrophic shift to a desert was preceded by clear spatial self-organization of the vegetation. However, several studies demonstrated the patterning itself can be relatively fluid and responsive to local conditions. At the same time, to our knowledge, there are not any studies that have investigated a system where patterns have emerged from previously un-patterned vegetation.

This research aims to understand the change and development of a banded vegetation pattern found in an arid region of the High Plains in Colorado (Figure 1). In order to study this site, we wanted to analyze the pattern from high-resolution aerial images from the years 1999-2019 to quantify if the observed specific vegetation patterns were significant and how they formed over time. Understanding the development and transition of these organized patterns could provide important insight into how past, current and future changes in the climate could potentially affect arid ecosystems globally. By analyzing natural spatial patterns, we aim to gather information on the significance, presence, strength, and orientation of the waves in each banded pattern in order to gain understanding of how these patterns are affected exogenously and endogenously in the plot studied in the High Plains (Penny et. al 2013).

Methods

2.1. Chico Basin Study Area

The site analyzed for specific vegetation patterns is found on the border between El Paso County and Pueblo County in Colorado at Chico Basin Ranch. The El Paso County region gets approximately 10-15 inches of precipitation annually (CO Airport). There were severe drought years in El Paso County during 2002, 2010 and 2012. Data show that average temperatures at a study site at the Pueblo Chemical Depot in Pueblo County (coordinates: 38.360426, -104.345081), approximately 18 km from the AOI at the Chico Basin Ranch, are increasing 0.06 C° per decade (Rondeau et. al, 2016).

The study site is a shortgrass prairie which is predominantly covered in a signature species of grass called Blue Grama (*Chondrosum gracile)*. Blue Grama grass is nutrient rich and an important food-source for cattle. However, from the years 1999-2015, the Colorado Natural Heritage Program noted a significant decline in Blue Grama populations (in El Paso County, several miles south of our study site) due to the drought years that occurred during their study. The population decreased 62% from 1999 to 2015 (Rondeau et. al, 2016), which led to the emergence of the specific vegetation bands that will be analyzed in this study (Sticpewich, 2021). Other dominant vegetation species include other varieties of perennials like the Buffalo grass (*Bouteloua dactyloides)* and the Cholla cactus (*Cylindropuntia*) (Foster, 2021).

The site used is a 2 km^2 plot located immediately east of the Chico Basin Ranch airstrip and approximately 61 km southeast of Colorado Springs, CO (coordinates: 38.513424, -104.418923). Images taken for analysis were collected from Google Earth aerial imagery for the years 1999, 2003, 2017 and 2019. As can be seen in Figure 1, the plot has several notable features. There is an airstrip on the western side of the plot which was constructed during the analysis period. There are also several cow trails and a watering hole that can be seen in each year. Since Chico Basin Ranch is a cattle ranch, it is important to note that the study site has

been impacted by grazing. The site contains specific banded vegetation patterns that are approximately 30 m long and 5 m wide. These banded vegetation patterns at Chico Basin have become more prevalent in the last five years.

2.2 Preparing Climate Data

The Colorado Climate Center provided the climate information collected for this study. The weather station is at the Colorado Springs Municipal Airport, which provides climate data from 1948-2022 of El Paso County. The Colorado Springs Airport (coordinates: 38°48'05.9"N 104°42'09.3"W) is located approximately 56 km northwest of the study site at Chico Basin Ranch. Data were extracted from an online database and uploaded into Excel for analysis (Figure 3).

2.3 Preparing Geospatial Imagery

Data were collected by taking several clippings from Google Earth high-resolution aerial imagery. The images taken from Google Earth had a resolution of 0.5-meter pixels. We used high-resolution imagery for fine-scale analysis and to be able to classify the differences between bare and vegetated patches (Penny et. al, 2013). The area studied in Chico Basin did not have high resolution imagery for every year. The majority of the years, half of the research plot did not have images taken of it. In the end, the years 1999, 2003, 2015, 2017, and 2019 were chosen since they had the high-resolution imagery available for the whole plot (Figure 1).

The imagery from Google Earth was then uploaded into ArcGIS Pro and prepared for further analysis in R Studio (V 1.2.5033). Each year was clipped to the 1 x 2 km plot and georeferenced to assure there was not any variance in location of the plot. The images were

classified using a two-class quantile classification based on total brightness. Darker patches that were vegetation were given the value of 1; whereas the bright, bare sections were given the value of 0. The upper values of the classification for each year were recorded and used in later analysis.

2.4 Data Analysis

2.4.1 Basic Theory for the Analysis of Compound Waves in Two Dimensions by Fast-Fourier Transform

A standard way of analyzing complex patterns is a Fast-Fourier Transform (FFT). An FFT takes images with recognizable patterns, which are products of a series of waves combined, and takes the pattern apart, extracts each individual cos and sin wave and gives the information on the characteristics of each wave found. The resulting product is a two-dimensional periodogram. Periodograms offer a more compact description of spatial patterns by showing the different frequencies, amplitudes, and orientations of the waves found in the pattern (Ford and Renshaw, 1984). Each wave is represented by a pair of signals that represent the direction, frequency, and amplitude of the wave. The frequency of the wave is distance from origin which is also known as the wave number. The amplitude of the wave is the value behind the pixel, shown as a color. It is at a gradient from blue to red, the red waves having the higher amplitudes. The direction of the wave is shown by the location of the wave on the periodogram. Figure 4 (*c)* shows the resulting periodogram of the FFT analysis for the propagating wave in Figure 4 (*b*).

Before the data could be entered into R Studio to be analyzed, several steps had to happen. Below are the annotated steps in the R Studio code used for the analysis. The *spectral*, *raster*, and *rgdal* packages are necessary for running the analysis. Patterns are a series of waves that are combined which each having its own orientation, magnitude and frequency. In order to

analyze the aerial imagery of the banded vegetation patterns, simple wave patterns needed to be made and analyzed first. This first section of code makes a periodic pattern in two dimensions where the waves are oriented at 45° with a frequency of 3 and an amplitude of 2 (Figure 4 (*a)*). The mathematical formula for a two-dimensional wave is

$$z = a * sin(2\pi * (fx)x + 2\pi(fy) * y$$

where a = amplitude and *fx/y* are the varying frequencies of *x* and *y*.

```
library(spectral)
library(raster)
library(rgdal)

x <- seq(0, 1, length.out = 100)
y <- seq(0, 1, length.out = 100)

# calculate the data
m <- matrix(0, nrow=length(x), ncol=length(y))
for (i in 1:length(x))
  for (j in 1:length(y))
    m[i, j] <- 2* sin(2 * pi* 3 * x[i] + 2 * pi *3* y[j])

#plotting the wave
rasterImage2(x = x,
             y = y,
             z = m,
             main = "Wave at 45°")
```

Periodic patterns can consist of waves in multiple directions. The code below shows the creation of a more complex pattern where three waves are combined. It combines a diagonal wave, similar to the code above, with a North-South wave and an East-West wave of varying amplitudes and frequencies Figure 4 (*b*).

```
x <- seq(0, 1, length.out = 100)
```

```
y <- seq(0, 1, length.out = 100)

# calculate the data
m <- matrix(0, nrow=length(x), ncol=length(y))
for (i in 1:length(x))
  for (j in 1:length(y))
    m[i, j] <- sin(2*pi*3*x[i] + 2*pi*3* y[j]) + sin(2*pi*0*x[i] + 2*pi*7*y[j]) + sin(2*pi*12*x[i]
+2*pi*0*y[j])

#plotting the wave
rasterImage2(x = x,
          y = y,
          z = m,
          main = "Propagating Wave")
```

Figure 4 *(c*) shows the periodogram for the propagating wave in Figure 4 (*b)* created by the code below. The periodogram produces results that are symmetrical at 0,0; meaning, if there is a peak at 90°, the peak will also show up on the periodogram reflected at 270°. This would create an analysis that is not accurate since there are two peaks associated to one wave. This issue is resolved by cutting the matrix in half and only using the upper half of the periodogram for analysis. After *fy* is cut in half, the *fx* and *fy* vectors, defined in the code below, are joined together to create a final matrix (I.for.analysis) that is the upper half of the original matrix.

```
FT <- spec.fft(x = x1, y = y1, z = m)
# plot
plot(FT,xlim = c(-15, 15), ylim = c(-15, 15))

fx<-FT$fx # x axis of periodogram
fy<-FT$fy # y axis of periodogram
I<-abs(FT$A) # raster image of periodogram

#I.for.analysis<-I[,51:100]
I.for.analysis<-I.final[,(1+.5*length(fy)):length(fy)]
```

There are several ways the FFT can be further analyzed. The waves can be extracted individually and the direction of the waves can be focused on through the theta spectrum. This splits the periodogram into slices, similar to that of a pie, and aggregates the signal within each slice (Figure 4 (*d)).* The aggregated signals are the degrees at which the orientation of the waves are trending. The angles go counterclockwise. Directly East is 0°, North is 90°, West is 180° and South is 260°.

```
fy.for.analysis<-fy[(1+.5*length(fy)):length(fy)]
theta.matrix<-matrix(NA,nrow=length(fx),ncol=length(fy.for.analysis))
dim(theta.matrix)
for (i in 1:length(fx)){
  for (j in 1:length(fy.for.analysis)){
    theta.matrix[i, j] <- (180/pi)*atan2(fy.for.analysis[j],fx[i])
  }}
image(theta.matrix)

ang.bin.size<-10 # how many degrees is each bin
ang.bin.number<-180/ang.bin.size #needs to be an integer
ang.bin.cutoffs<-seq(from=0,to=180,by=ang.bin.size)
#ang.bins are the centers of the ang bin cut offs for plotting
ang.bins<-(ang.bin.cutoffs[1:(length(ang.bin.cutoffs)-
1)]+ang.bin.cutoffs[2:(length(ang.bin.cutoffs))])/2

ang.bin.cell.counter<-numeric(length = ang.bin.number) #records the number of pixels in each
bin
ang.bin.aggregated.signal<-numeric(length = ang.bin.number) #records the sum of values of all
pixels counted in each bin

####actual theta spectrum analysis####
for (a in 1:ang.bin.number){
  for (i in 1:length(fx)){
    for (j in 1: length(fy.for.analysis)){
      if(theta.matrix[i,j]>=ang.bin.cutoffs[a]&theta.matrix[i,j]<ang.bin.cutoffs[a+1]){
        ang.bin.cell.counter[a]<-ang.bin.cell.counter[a]+1
        ang.bin.aggregated.signal[a]<-ang.bin.aggregated.signal[a]+I.for.analysis[i,j]
      }}}}
ang.bin.averaged.signal<-ang.bin.aggregated.signal/ang.bin.cell.counter
plot(ang.bins,ang.bin.averaged.signal,type="l")
```

The wavelength signal can also be interpreted. This is done using the radial spectrum analysis. The radial analysis aggregates signals that share the same frequency into rings of concentric circles. The orientation of the signals is not accounted for. The signals show the wavelengths that are present in the pattern. In the code, each ring is isolated so that the number of cells can be counted and the signals can be aggregated. This produces a radial spectrum graph that peaks at each wave frequency (Figure 4 *(e)*).

```
##Radial spectrum
radial.matrix<-matrix(data=0,nrow=length(fx), ncol=length(fy))

#calculates the distance of each pixel from the center
for (i in 1:length(fx)){
  for (j in 1:length(fy)){
    radial.matrix[i, j] <- ((fx[i]^2)+(fy[j])^2)^0.5 #calculates the distance of each pixel from
thecenter
  }}
image(radial.matrix) #mid-processing check

r.max<-round(max(radial.matrix)) #this is the maximum wave number (frequency) that is
detectable
#here r.max is 70 when rounded (distance to the corners)
r.max<-70
r.bin.size<-1
r.bin.number<-r.max/r.bin.size #=70
r.bin.cutoffs<-seq(from=0,to=r.max,by=r.bin.size)
r.bins<-(r.bin.cutoffs[1:(length(r.bin.cutoffs)-1)]+r.bin.cutoffs[2:(length(r.bin.cutoffs))])/2

####actual radial spectrum analysis####
r.bin.cell.counter<-numeric(length = r.bin.number) #records the count of the number pixels per
bin (as we move out, the number of pixels increases)
r.bin.aggregated.signal<-numeric(length = r.bin.number) #records the sum of  values of pixels in
each bin
for (a in 1:r.bin.number){
  for (i in 1:length(fx)){
    for (j in 1: length(fy)){
      if(radial.matrix[i,j]>=r.bin.cutoffs[a]&radial.matrix[i,j]<r.bin.cutoffs[a+1]){
        r.bin.cell.counter[a]<-r.bin.cell.counter[a]+1
        r.bin.aggregated.signal[a]<-r.bin.aggregated.signal[a]+I.final[i,j]
```

```
    }}}}

r.bin.averaged.signal<-r.bin.aggregated.signal/r.bin.cell.counter
```

3.2.2 Site Imagery Analysis

The 1x2 km clips from ArcGIS Pro were uploaded into R Studio. The images acquired from ArcGIS were adjusted to an 8-bit grey scale in preparation to upload them into R. The code below creates a raster of the 1x2 km plot from the 8-bit grey scale images made in ArcGIS. The raster created in the code is from the image of the 1x2 km plot in 2017. The 2017 raster is loaded into an automation which analyzes the raster by cutting out 80 m tiles of the image and running an FFT analysis, as explained above, on them. The entire 1x2 km plot is analyzed in a series of 80 m tiles which provides information on the characteristics of the significant waves in the patterns of each tile. This automation will examine the plot for each year available.

```
AOI.tiff<- raster("AOI_2017_clip.tif")
AOI.tiff
plot(AOI.tiff)
```

The image of the area of interest (AOI) undergoes a two-step classification based on the upper values from the quantile classification extracted from ArcGIS Pro. For example, with the 8-bit (ranging 0 – 255) grey scale image of the AOI in 2017, any values less than 109 are replaced with zero and any values greater than 109 with one. This creates an image with two values. This is required in order to run the FFT analysis on the images of the AOI. The upper values are different for each year. The AOI is then made into an isolated matrix, which removes extra geospatial information that is not needed.

```
# upper values for 2019:110, 2017:109, 2015:90, 2003:121, 1999:87
r.mat<-c(-Inf,109,0,109,Inf,1)
rclmat<-matrix(r.mat, ncol=3, byrow=TRUE)
AOI.tiff<-reclassify(AOI.tiff, rclmat)

#extracting the matrix that codes the image
mat.AOI.tiff<- as.matrix(AOI.tiff)
```

The code automates the extraction and analysis of each 80 m tiles in the 1x2 km AOI to determine if patterns are present. There was an exploration of tile sizes before deciding that 80 m fit the best. This is because waves come at different sizes, and different patterns would be recognized depending on the size of the tile. We elected 80 m to be the tile size after exploring 60 m, 80 m, 100 m, 120 m and 140 m tiles. 80 m tiles maximized the algorithm's ability to find waves, as shown in Figure 5. The 1x2 km clip was trimmed to in order to be divisible by 80 m. The trimmed AOI matrix was then rotated to the correct orientation, where North on the clip corresponded to 90° with respect with to the *x* axis.

```
tile.size<-80*2 #this is in number of pixels, we have 0.5m pixels
k<-dim(mat.AOI.tiff)[1]
k # number of rows
l<-dim(mat.AOI.tiff)[2]
l # number of columns
new.row<-trunc(k/tile.size)*tile.size
new.row
new.col<-trunc(l/tile.size)*tile.size
new.col

#trim clip to make it (1x2km) divisible by tile size
mat.AOI.tiff<-mat.AOI.tiff[1:new.row,1:new.col]

#rotating the matrix so when plotted North in north
rotate <- function(x) t(apply(x, 2, rev))
AOI<-rotate(mat.AOI.tiff)
```

A portion of the code that cut a test tile out of the AOI was implemented before the automation ran in order to assure the code was functioning properly. Additionally, x and y coordinates were created for the image and the analysis. The coordinates started at 0,0 in the upper right corner of the tile. There are 25 rows and 12 columns to the AOI clip.

```
i<-6 # i goes to 25
j<-6 # j goes to 12
tile.ij<-AOI[((tile.size*i-tile.size)+1):(tile.size*i),((tile.size*j-tile.size)+1):(tile.size*j)]

x <- seq(0, 1, length.out = dim(tile.ij)[1])
length(x) #must be the same as number of rows in the image matrix
y <- seq(0, 1, length.out = dim(tile.ij)[2])
length(y) #must be the same as number of columns in the image matrix
```

Several parts of the code are repeating parts of the analysis that could be kept out of the automation. Most of this code defines characters that will repeat as the same value each time the FFT is run on a different 80 m tile of the plot. This includes cutting the periodogram matrix in half to prevent symmetrical wave peaks and creating empty matrices with the same dimensions as the matrix cut in half to input theta and radial spectrum values. Angles are corrected so zero is pointing east in the theta matrix in order to identify proper orientation values for the theta spectrum analysis. The sister matrix created for the radial spectrum analysis populates each cell with their distance from 0,0. The rest of the repeating parts are important cutoff values that define the bin sizes of the theta and radial analyses.

```
FT<-spec.fft(x = x, y = y, z = tile.ij)
fx<-FT$fx
fy<-FT$fy

fy.for.analysis<-fy[(1+.5*length(fy)):length(fy)]
```

```
theta.matrix<-matrix(data=0,nrow=length(fx),ncol=length(fy.for.analysis))
radial.matrix<-matrix(data=0,nrow=length(fx),ncol=length(fy.for.analysis))

#calculating angles for the theta matrix .... zero is pointing east
for (i in 1:length(fx)){
  for (j in 1:length(fy.for.analysis)){
    theta.matrix[i, j] <- (180/pi)*atan2(fy.for.analysis[j],fx[i])
  }}

#populating the radial matrix with distances from the (0,0) on fx and fy vectors
for (i in 1:length(fx)){
  for (j in 1:length(fy.for.analysis)){
    radial.matrix[i,j] <- ((fx[i]^2)+(fy.for.analysis[j])^2)^0.5
  }}

### setting angular bin size cutoffs ###
ang.bin.size<-5
ang.bin.number<-180/ang.bin.size
ang.bin.cutoffs<-seq(from=0,to=180,by=ang.bin.size)

### setting radial bin size cutoffs ####
r.max.mk<-20
r.bin.size<-1/3 #bin sizes are adjusted here
r.bin.number<-r.max.mk/r.bin.size #figuring out how many bins we have
r.bin.cutoffs<-seq(from=0,to=r.max.mk,by=r.bin.size)
```

The last repeating section of the code is called the ‘doughnut’. This is an integral part of the analysis. The ‘doughnut’ is first created by making an empty matrix with the dimensions of *fx* and *fy*. For each 80 m tile that is examined in the FFT automation, any values less than one and greater than 12 in the periodogram produced by the FFT will be replaced with zero. The result is a periodogram which only records values between one and twelve, resembling a doughnut. The cutoff values are important and the doughnut needs to be of an appropriate size in order to recognize the relevant patterns (Penny et. al, 2013). The doughnut was first applied to three different 80 m tiles of the AOI as an exploration to determine the appropriate cutoff values. One tile did not have any recognizable banded vegetation patterns, the next had a mix of banded

patterns and patchiness and the last tile had a significant amount of banded vegetation patterns. The banded vegetation patterns consist of wavelengths that repeat every 10-15 meters. Any wavenumbers larger than 12 would analyze noise-like variability at the level of individual patterns. Wavenumbers of 1 would be the dominant wavelength. This is because anytime there is a gradient-like pattern in the image, the densest sections will create significant wavelengths of one. After the exploration, it was decided that the cutoff values of 1 and 12 removed any static and waves that would undermine the analysis.

```
doughnut<-matrix(data=0,nrow=length(fx), ncol=length(fy))
for (i in 1:length(fx)){
  for (j in 1:length(fy)){
    doughnut[i, j] <- ((fx[i]^2)+(fy[j])^2)^0.5 #calculates data of pixels from each direction ie
distance from center
  }}
doughnut[doughnut <=1] <-0
doughnut[doughnut >=12] <-0
doughnut[doughnut >1 & doughnut <12] <-1 #replace numbers between 1 and 12 with 1
```

Empty matrices were also created to put the results of the automation into. The results include the radial spectrum, the theta spectrum and the dominant wave for each 80 m tile, which appropriate empty matrices have been made for.

```
### Define output matrices ###
# R.mat is an empty matrix to put our r-spectrum (peak wave) data into
# If smaller than statistically significant cut off value, values will be zero
R.mat<-matrix(data=0,nrow=dim(AOI)[1]/tile.size,ncol=dim(AOI)[2]/tile.size)
#R.mat

# Th.mat is an empty matrix to put our theta-spectrum (dominant orientation) data into
Th.mat<-matrix(data=0,nrow=dim(AOI)[1]/tile.size,ncol=dim(AOI)[2]/tile.size)

# Dominant wave matrix
W1.wave.number <-matrix(data=0,nrow=dim(AOI)[1]/tile.size,ncol=dim(AOI)[2]/tile.size)
```

```
W1.dir<-matrix(data=0,nrow=dim(AOI)[1]/tile.size,ncol=dim(AOI)[2]/tile.size)
W1.pc.var<-matrix(data=0,nrow=dim(AOI)[1]/tile.size,ncol=dim(AOI)[2]/tile.size)
```

After all repeating parts of the code are defined, the automation for the analysis can be run. The automation is a large for-loop which analyzes the entire 1x2 km AOI in 80 m increments for the orientation, wavelength and dominant wave of the pattern in each tile. The theta and radial spectrum in the for-loop also are compared against a confidence interval (in the code: qchisq()) that assures the values are statistically significantly different from complete spatial randomness (Ford and Renshaw, 1984). The result is a culmination of analyses which show the presence of the banded vegetation patterns of the given year. The code was applied to rasters of the years 1999, 2003, 2015, 2017 and 2019. It begins by cutting an 80 m tile out of the plot starting at (0, 0). After the analysis is run on one 80 m tile, the next tile is cut out and the analysis is run again on the new tile. The analysis runs until the last tile is cut out at the bottom right corner, (12, 25), on the 1x2 km plot. After the tile is cut out, the FFT is ran on the tile. The doughnut is placed on the periodogram created by the FFT and the lower half of the periodogram is thrown out. Only the pixels in the doughnut are analyzed. Theta spectrum, radial spectrum and dominant wave analyses are run and the results for the tile are placed into the empty matrices (Th.mat, R.mat, W1.dir, W1.pc.var & W1.wave.number) created earlier.

```
### Automation ###
dim(R.mat) # setting up the loop that fills the matrix
dim(AOI)
r.row<-dim(R.mat)[1]
c.col<-dim(R.mat)[2]

for(r in 1:r.row) { # r = rows
  for(c in 1:c.col) { # c = columns
   #cutting the tile
```

```
   tile<-AOI[((tile.size*r-tile.size)+1):(tile.size*r),((tile.size*c-tile.size)+1):(tile.size*c)] #cutting
the tile

   #centering tile
   mean.tile <- mean(tile)
   tile<-tile-mean.tile
   #running the FFT
   FT<-spec.fft(x = x, y = y, z = tile)
   I<-abs(FT$A) #extracting the periodogram matrix
   #calculating variance
   mean.tile <- mean(tile) #calculate mean
   tile.prime <-tile-mean.tile #calculating departures from the mean
   tile.prime.squared <- tile.prime^2 #gets rid of negatives and shows stronger values
   sum.squares <- sum(tile.prime.squared) #add squares together
   variance.tile <- sum.squares/(dim(tile)[1]*dim(tile)[2]) #divide by sample size
   #adjusting periodogram matrix by the variance
   I.mr <- (dim(tile)[1]*dim(tile)[2])*I^2
   I.final <- I.mr/variance.tile
   #I.final<-I^2
   I.final<-I.final*doughnut
   #throw away the bottom half of the periodogram
   I.for.analysis<-I.final[,(1+.5*length(fy)):length(fy)]
   fy.for.analysis<-fy[(1+.5*length(fy)):length(fy)]
   # sets the angular analysis vectors
   ang.bin.cell.counter<-numeric(length = ang.bin.number) #counts number of pixels
   ang.bin.aggregated.signal<-numeric(length = ang.bin.number) #sum of values of all pixels
   #ang.bins are the centers of the ang bin cut offs for plotting
   ang.bins<-(ang.bin.cutoffs[1:(length(ang.bin.cutoffs)-
1)]+ang.bin.cutoffs[2:(length(ang.bin.cutoffs))])/2
   for (a in 1:ang.bin.number){ #180/10
     for (i in 1:length(fx)){ #length of x-axis
       for (j in 1: length(fy.for.analysis)){ #length of y-axis
         if(theta.matrix[i,j]>=ang.bin.cutoffs[a]&theta.matrix[i,j]<ang.bin.cutoffs[a+1]){
           if(I.for.analysis[i,j]>0){ang.bin.cell.counter[a]<-ang.bin.cell.counter[a]+1}
           ang.bin.aggregated.signal[a]<-ang.bin.aggregated.signal[a]+I.for.analysis[i,j]
         }}}}
   ang.interval<- (1/(2*ang.bin.cell.counter))*qchisq(.99999, df=ang.bin.cell.counter*2) #
confidence interval from Renshaw and Ford (1984)
   ang.bin.avg.signal<-ang.bin.aggregated.signal/ang.bin.cell.counter
   ang.max<-max(ang.bin.avg.signal) # value of the peak
   ang.max.index<-which.max(ang.bin.avg.signal)
   ang.max.location<-ang.bins[ang.max.index]
   ang.max.interval.cutoff<-ang.interval[ang.max.index]
   if(ang.max>ang.max.interval.cutoff){Th.mat[r,c]<-ang.max.location} else {Th.mat[r,c]<-(-
999)}
```

```
   # radial analysis set up
   r.bin.cell.counter<-numeric(length = r.bin.number) #counts number pixels per bin (as we
move out, the number of pixels increases), how many elements/bins are in each element of the
radial bin
   r.bin.aggregated.signal<-numeric(length = r.bin.number) #sum on values of pixels
   r.bins<-(r.bin.cutoffs[1:(length(r.bin.cutoffs)-1)]+r.bin.cutoffs[2:(length(r.bin.cutoffs))])/2

   for (b in 1:r.bin.number){
     for (k in 1:length(fx)){
       for (l in 1:length(fy.for.analysis)){
         if(radial.matrix[k,l]>=r.bin.cutoffs[b]&radial.matrix[k,l]<r.bin.cutoffs[b+1]){
           if(I.for.analysis[k,l]>0){r.bin.cell.counter[b]<-r.bin.cell.counter[b]+1}
           r.bin.aggregated.signal[b]<-r.bin.aggregated.signal[b]+I.for.analysis[k,l]
         }}}}
   r.interval<- qchisq(.99999, df=(r.bin.cell.counter))
   r.interval[is.na(r.interval)] <- 0
  # r.bin.avg.signal<-r.bin.aggregated.signal/(r.bin.cell.counter)
   r.bin.aggregated.signal[is.na(r.bin.aggregated.signal)] <- 0
   r.max<-max(r.bin.aggregated.signal) # value of the peak
   r.max.index<-which.max(r.bin.aggregated.signal)
   r.max.location<-r.bins[r.max.index]
   r.max.interval.cutoff<-r.interval[r.max.index]
   if(r.max>r.max.interval.cutoff){R.mat[r,c]<-r.max.location} else {R.mat[r,c]<-(-999)}

   ########## Dominant Wave
   I.2<-I^2
   I.2<-I.2*doughnut
   I.pc.variance<-100*(I.2/variance.tile)
   I.pc.variance_TopHalf<-I.pc.variance[,(1+.5*length(fy)):length(fy)]
   correction.mat<-matrix(data=1,nrow=length(fx),ncol=length(fy.for.analysis))
   correction.mat[1:(1+(0.5*length(fx))),1]<-0 #replace top half of first half of column with 0
   I.pc.variance_TopHalf<-I.pc.variance_TopHalf*correction.mat
   ###finding the frequency and direction of the wave with the largest amplitude.
   max1.location<- which(I.pc.variance_TopHalf == max(I.pc.variance_TopHalf), arr.ind =
TRUE)
   #find the percent of variance explained by the largest wave and compare to cut offs above
   W1.pc.var[r,c]<-I.pc.variance_TopHalf[max1.location[1],max1.location[2]]
   ### translate the location to x-y coordinate of the periodogram (remembering that each wave
is represented by two points)
   max1.XY<-c(fx[max1.location[1,1]],fy.for.analysis[max1.location[1,2]])
   #Wave number
   W1.wave.number[r,c]<-(max1.XY[1]^2+max1.XY[2]^2)^(0.5) #write this down
   #direction of the largest wave in degrees (east=0)
   W1.dir[r,c]<-(180/pi)*atan2(max1.XY[2],max1.XY[1])
   }
}
```

The final section of the code extracts the information in the newly filled matrices and prepares the results. An exploration of wavelengths had to be conducted before a cutoff value for statistically significant banded vegetation patterns could be defined and appropriate figures made. According to Penny et. al (2013), the wavelength cutoff chosen improves the ability for the radial spectrum analysis to recognize appropriate pattern. In their study, they chose a cutoff value of 5, meaning that the wave had to repeat at least five times within the tile in order to the banded pattern to be statistically significant. However, their tiles were 120x120 m and banded patterns generally repeated every 20 meters at their AOI. Our AOI is 80x80 m and banded patterns repeat about every 10 meters. Therefore, we explored wavenumber cutoff values of 4 and 5 (Figure 5). We concluded a wavenumber of 4 was the appropriate value to optimize recognition of the statistically significant banded patterns found by the radial spectrum analysis. The radial spectrum analysis was then reviewed and percentages of statistically significant banded vegetation patterns and percentages of dominant waves for each year in the AOI was made. The theta spectrum results were converted into compass degrees. The results were then created into Figures 6-8.

```
R.mat
image(R.mat) # where all of the patterns are

#simplifying Rmat
R.mat.4<-0*R.mat
R.mat.4
for(r in 1:r.row) { # r = rows
  for(c in 1:c.col) {
    if(R.mat[r,c]>4){R.mat.4[r,c]<-1} else {R.mat.4[r,c]<-0}
  }}
image(R.mat.4)
sum(R.mat.4)
```

```
49/(dim(R.mat.4)[1]*dim(R.mat.4)[2]) #percentage statistically significant banded patterns present in AOI

#wave number
W1.wave.number.4<-0*W1.wave.number
W1.wave.number.4
for(r in 1:r.row) { # r = rows
  for(c in 1:c.col) {
    if(W1.wave.number[r,c]>4){W1.wave.number.4[r,c]<-1} else {W1.wave.number.4[r,c]<-0}
  }}
image(W1.wave.number.4)
sum(W1.wave.number.4
22/(dim(W1.wave.number.4)[1]*dim(W1.wave.number.4)[2]) #percentage dominant waves in AOI

### averaging angles for orientation graph
Th.mat.sin<-sin((pi/180)*Th.mat)
mean.sin<-mean(Th.mat.sin)
Th.mat.cos<-cos((pi/180)*Th.mat)
mean.cos<-mean(Th.mat.cos)
(180/pi)*atan2(mean.sin,mean.cos) # in radians

W1.dir.sin<-sin((pi/180)*W1.dir)
mean.W1.sin<-mean(W1.dir.sin)
W1.dir.cos<-cos((pi/180)*W1.dir)
mean.W1.cos<-mean(W1.dir.cos)
(180/pi)*atan2(mean.W1.sin,mean.W1.cos) # in radians
```

Results

4.1 Analysis of climate over time

The data collected from the Colorado Climate Center provided insight into climate patterns at the Colorado Springs Airport over a 70-year study period. Noticeable temperature maxima changes began during 1995~2005, which suggests that the regime shift occurred around then. Figure 3 shows annual averages from daily minimum/maximum temperatures and precipitation data collected from the weather station at the airport. Temperature maxima in Figure 3 *a/b* show an important shift in the climate regime in El Paso County. Temperature maxima (*a*) show an

upward linear trend that minima (*b*) has a consistent upward linear trend for the 70-year record. The precipitation data (Figure 3 *c/d)* do not show a distinct linear trend and would require a regime shift analysis, which is beyond the scope of this thesis. However, they do show evident droughts that took place in 2002, 2010 and 2012. The driest year on record was 2002, in which the airport received 7.85 in of precipitation. 2012 was the second driest year, at 8.11 in, and 2010 the fourth driest, at 9.37 in. These significant droughts can also be seen in the temperature data as well. Three out of the four strongest droughts in the 70-year record happened during a 20-year period from 1999-2019 which coincides with the period of observation for this study.

4.2 Fast Fourier Transform Results

The automated code provided several results about the banded vegetation patterns in the study plot from 1999 – 2019. To begin, the proportion of the AOI with banded patterned tiles has increased over time. Figure 7 shows the upward linear trend in the increased development of significant banded vegetation patterns in the AOI from 1999 to 2019. These results are complemented with Figure 6, which shows the trend visually. In 1999, the pattern was present in 14.7% of the plot; whereas, in 2019, 36% of the plot contained the pattern. The radial spectrum analysis on these plots also revealed the presence of dominant waves in each AOI. The results show the number of dominant waves in the study plot, which increased from 3.7% in 1999 to 22.3% in 2019. The theta spectrum analysis concluded the orientation of the banded vegetation patterns generally face North (90°) and the orientation of the pattern was already established when the tiles consisted mostly of aperiodic patchiness (Figure 8). Qualitatively, the pattern orientation is congruent with the slope (Figure 9). The slope of the AOI declines at a N-S orientation and there is not a slope in the E-W direction.

Significant periodic anisotropic patterns are present at Chico Basin Ranch in all years analyzed. Figure 6 shows the portion of the 1999 AOI with 80 m tiles that contain significant banded vegetation patterns that have a wavelength greater than 4 meters (*a)* compared to a map of tiles in 1999 that contains all patterns found (*c)*. The AOI during 1999 is not completely spatially random. The tiles that did not contain statistically significantly different from complete spatial randomness and were anisotropic. The radial spectrum analyses for the tiles were completely different when compared to results from a plot that was completely spatially random.

Discussion

With climate change shifting temperature regimes to hotter and drier climates overall, arid ecosystems are expected to shift into a pattern state. Global and local changes in precipitation and an increase in risk of desertification have been observed due to climate change. This should drive pattern formation in arid grasslands due its effect on the availability of water. Patterning should increase water efficiency. Continued climate change could further drive the pattern formation at arid grasslands, increasing their water use efficiency and overall resiliency. However, banded vegetation patterns could also be seen as a forewarning to climate-induced desertification.

The climate in Chico Basin is trending to be drier and hotter. The average daily minima and maxima show an upward linear trend and point out a shift in temperature regime (Fig. 3 *a/b*). It is important to note the minima temperatures show a consistent upward linear trend during the entire 70-year record, while an upward linear trend appears in the temperature maxima data in the last 20-year recorded period of data for the Colorado Springs airport. Qualitative analysis suggests the onset of this trend began around 1995~2005 for El Paso County. Temperatures in Chico Basin are rapidly increasing. The precipitation data does not show a distinct linear trend

(Figure 3, *c/d*). However, they do suggest in the last 20 years, the variability of precipitation in El Paso County has shifted to having stronger droughts. The data show three out of the four most significant droughts of the 70-year record occurred during our 20-year period of study (in 2002, 2010 and 2012). The strongest drought on record occurred during 2002, where the Colorado Springs airport received 7.85 inches of rainfall, about 50% of their normal average annual precipitation. This is significant finding even though there is not a clearly defined regime shift for precipitation. The combined effects of an upward linear trend in temperatures and more substantial drought years have a significant consequence on evaporation rates in El Paso County. Higher evaporation rates could encourage a positive feedback between diminished water availability and decreased vegetation cover (Noy-Meir, 1973). The temperature regime shift and substantial drought years have happened during the 20-year period of our study and subsequently affected the proportion of statistically significant banded vegetation patterns at the AOI.

Periodic anisotropic patterns are currently found at Chico Basin Ranch. Visual analysis on Google Earth has shown the presence of these banded vegetation patterns. The FFT analysis on the study plot in Chico Basin Ranch demonstrates the banded patterns are present and statistically significant. The results show that the 1x2 km AOI at Chico Basin Ranch has a higher coverage of periodic anisotropic banded vegetation patterns in 2019 than it did in 1999. There was a substantial increase in the formation of periodic anisotropic patterns in the years after considerable droughts in the 20-year period of study. As shown in the 1999 analysis, significant banded patterns were present at low proportions of the AOI (14.7%) before the most substantial drought of the 70-year record which occurred in 2002. There was a delayed reaction in the formation of more patterns after 2002. In 2003, the AOI had 16.3% significant banded patterns; whereas, in the next available year (2015), significant patterns were present in 38% of the AOI

(Figure 7). This delay could be attributed to vegetation in the arid grasslands having their own resources stored up that could be used for a period of time in order to not respond immediately to the 2002 drought. However, as temperatures continued to increase and two more significant droughts occurred, banded vegetation patterns expanded considerably. Between 1999 and 2019, there was a 21.3% increase in the coverage of statistically significant banded patterns (Figure 7). There has not been a significant drought since 2012, and the patterns in 2015, 2017 and 2019 stay more consistent. This could be because since the banded vegetation patterns are established, they became a stable part of the landscape or the temperature regime is further concreting the patterns into the AOI.

Another important finding from the FFT analysis is the areas that do not have significant periodic patterns in the AOI are still statistically significantly different from complete spatial randomness (CSR). Initially, we expected the arid grassland at Chico Basin Ranch to be a homogenous landscape that developed periodic anisotropic patterns over time. The quantitative models created in others studies start their explorations with a fully spatially random landscape (Reitkerk et. al, 2004). However, as seen in the 1999 results, the landscape began with aperiodic anisotropic patchiness. The FFT explorations of all of the tiles found patterns that statistically significantly differed from CSR; however, not all of the dominant wavelengths were greater than 4, meaning that they were not within the commonly defined constraints of banded periodic patterns (Penny et. al, 2013). The low dominant wavenumbers signify a high degree of patchiness (Ford and Renshaw, 1984). Therefore, originally the landscape was patchy and anisotropic but not periodic; much of the landscape in 2019 still retains this character.

The patchy anisotropic vegetation structure could be explained by several mechanisms similar to those that drive the formation of periodic pattern formation. Periodic patterns form

from spatial coupling of positive feedbacks that lead to short-distance facilitation and long-distance inhibition. However, spatial patchiness can originate from positive feedbacks without the spatial coupling. Primarily, the positive feedback between infiltration and root density. The greater the root density, the higher the infiltration rate, the more water vegetation can absorb, which furthers the root depth and density and so forth. The positive feedback could also proceed in the opposite direction and further inhibit infiltration which inhibits plant growth, leading to an area of bare ground. Whether the positive feedback will lead to a patch of vegetation or a patch of bare ground depends on the initial vegetation density. Where initial vegetation density is above the threshold, commonly known as an Alee point, the patch will develop full vegetation coverage compare to when the initial vegetation density is below the Alee point. Hence, simple facilitation on landscapes allows patchiness to develop. The aperiodic anisotropic patchiness was present before the 2002 drought occurred, but the drought most likely encouraged the spatial coupling, resulting in short-distance facilitation and long-distance inhibition where the vegetation patches substantially depleted water from the bare patches.

The orientation of the patchy anisotropic vegetation structure appeared to be stable over time through the development of the periodic patterns (Figure 8). The orientation of the structures remained approximately N-S (about 90° counterclockwise from East). Overall, the AOI slopes predominantly from North to South at a slight decline (Figure 9). The patchiness, regardless if it is aperiodic or periodic, follows the slope contour lines. This suggests that the aperiodic patchiness most likely resulted from intercepting runoff.

The key finding of the present study is that the proportion of statistically significant banded vegetation patterns have increased in the 20-year period of study in response to three strong droughts and a sharp increase in annual temperatures. Previous studies have observed

changes in the width and spacing of pre-existing periodic vegetation patterns in response to changes in rainfall regime (Dunkerley et. al, 2018). With a decline in precipitation, there is an increase in the ratio of the run-off zone and the infiltration zone (Dunkerley et. al, 2018). The bare intergrove bands expanded while the vegetated grove bands shrank during years where there the annual rainfall was decreased. Thicker intergrove sections compensate for the lack of water (Valentin and d'Herbés, 1999). In the years of drought, vegetation cover decreases significantly and sometimes leads to desertification (Holmgren et. al, 2001). Previously, there had not been a study looking at an arid landscape with a low proportion of patterns and their development over time. Additionally, this study observed the formation of periodic patterns develop from patchy anisotropic aperiodic vegetation structures. Observing the formation of statistically significant banded vegetation patterns over time from a homogenous, random landscape could provide important insight into the mechanism behind these patterns and what they could mean for the future of arid ecosystems.

Quantitative models have concluded that the presence and formation of specific periodic vegetation patterns could coincide with a sudden catastrophic shift to a stable, bare homogenous landscape (Reitkerk et. al, 2004). However, findings of several local studies conducted on sites with banded vegetation patterns have contradicted the conclusions of quantitative models. In the study of the Broken Hill region, a semi-arid landscape in Australia, it was found that severe drought did not create the irreversible change of a vegetated landscape to a uniform bare landscape (Dunkerley et. al, 2018). The banded vegetation patterns did not die off, as predicted by quantitative models, like that of Reitkerk et. al (2004) and Vega & Montaña (2011), which concluded previously that an increased decline in rainfall and imposed grazing on an arid landscape would create homogenous bare landscapes.

It is necessary to keep in mind that the arid landscapes at Chico Basin Ranch, and in general, are used for grazing. Grazing can play an important role in how the landscape responds to water shortage. The effect of grazing on these ecosystems has had irreversible consequences on arid ecosystems in numerical models; however, it has not been studied enough empirically at a local scale to make conclusions of its effect on the stability of actual landscapes. Grazing management, especially during years of drought, could play a significant role in maintaining the resiliency of heterogeneous arid ecosystems (Reitkerk et. al, 1997). The timing and intensity of grazing at Chico Basin Ranch could be used as a management tool to help make an ecosystem more resilient from a rancher's perspective. In a spatially explicit mathematical model, decreased grazing could decrease pattern formation (Vega and Montaña, 2011), the link between grazing and pattern formation is currently poorly understood. Further local studies on how grazing impacts patterns and water-use efficiency could increase the understanding of specific vegetation patterns. Local study areas have unique factors that can influence the resiliency of a landscape, like the plant physiology or topography of the studied landscape. It is these discoveries from localized studies that further the understanding of spatial vegetation patterns.

Figures

a.

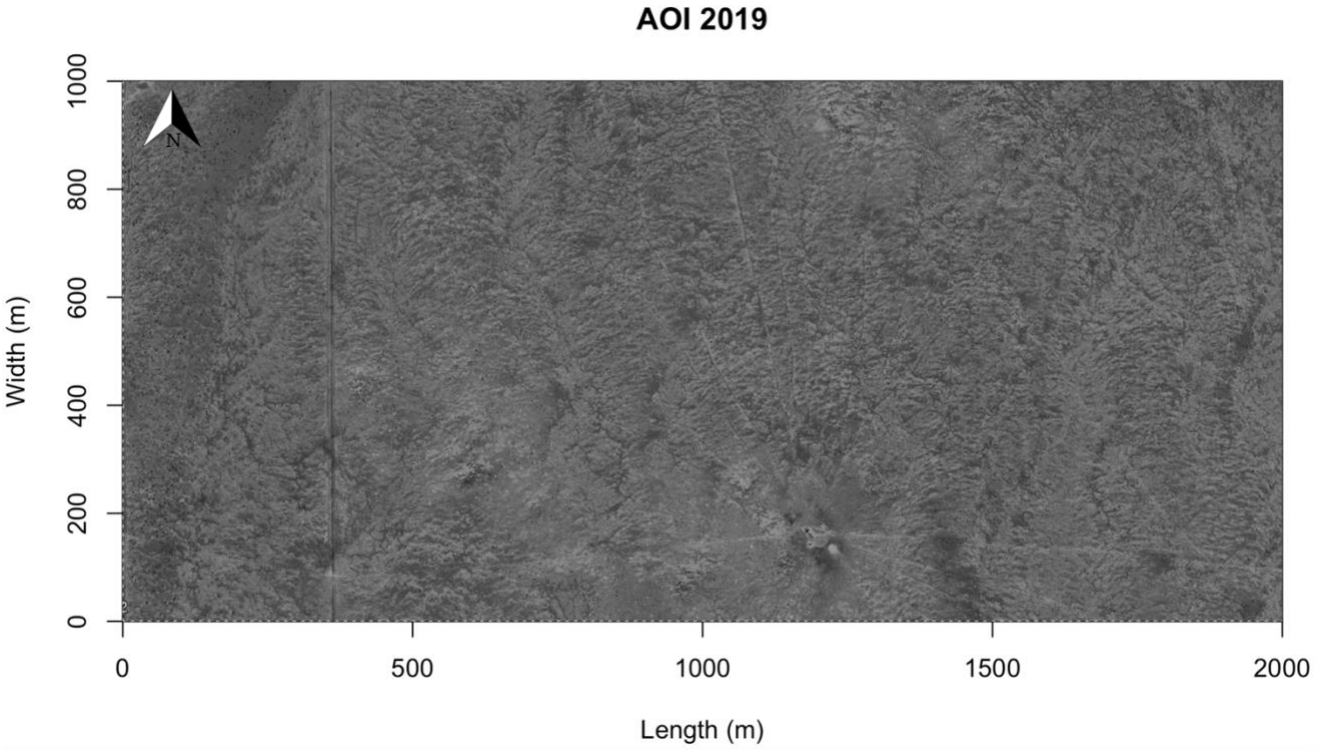
AOI 2019
N
Width (m)
0
200
400
600
800
1000
0
500
1000
1500
2000
Length (m)

b.

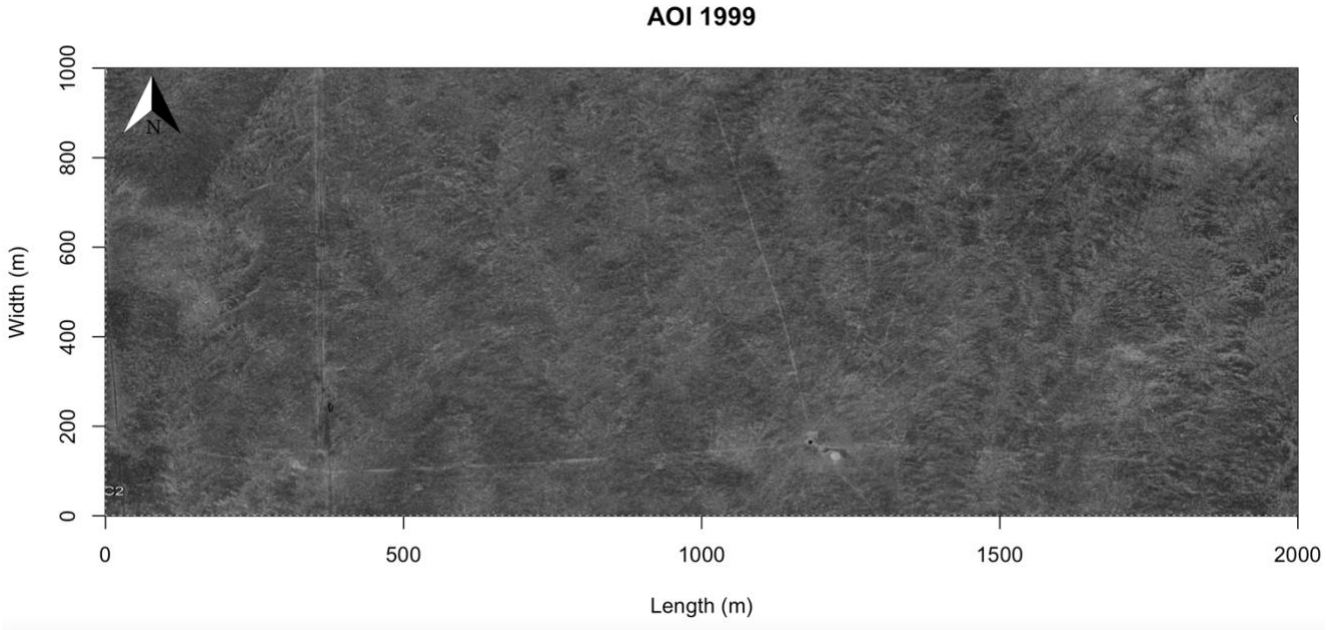
AOI 1999
N
Width (m)
0
200
400
600
800
1000
0
500
1000
1500
2000
Length (m)

Figure 1. The 1000x2000 m AOI at the Chico Basin Ranch, CO for the years 2019 (*a*) and 1999 (*b*). There are also 1x2 km study plots for the years 1999, 2003, 2015, and 2017. Darker colors indicate higher density of vegetation.

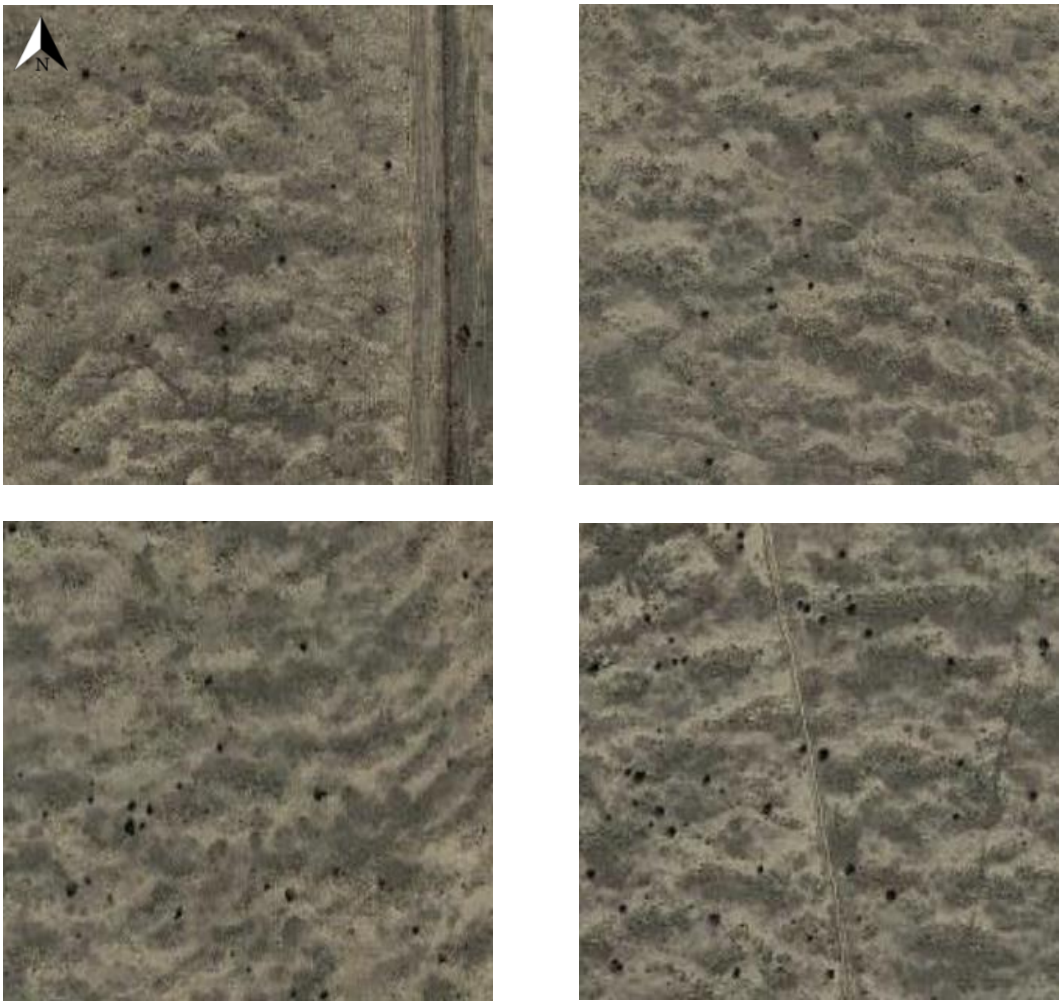

Figure 2. Google Earth images in 2019 of the banded vegetation patterns present at the 1x2 km study plot at the Chico Basin Ranch, Colorado. Each image is 100x100 m.

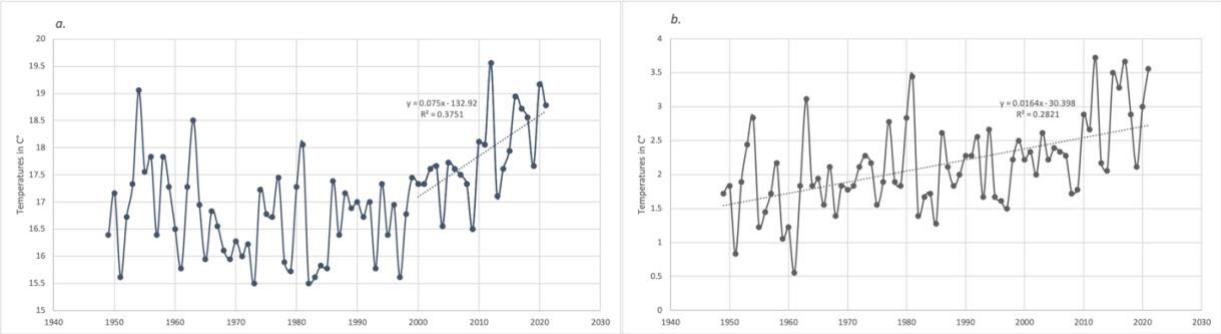

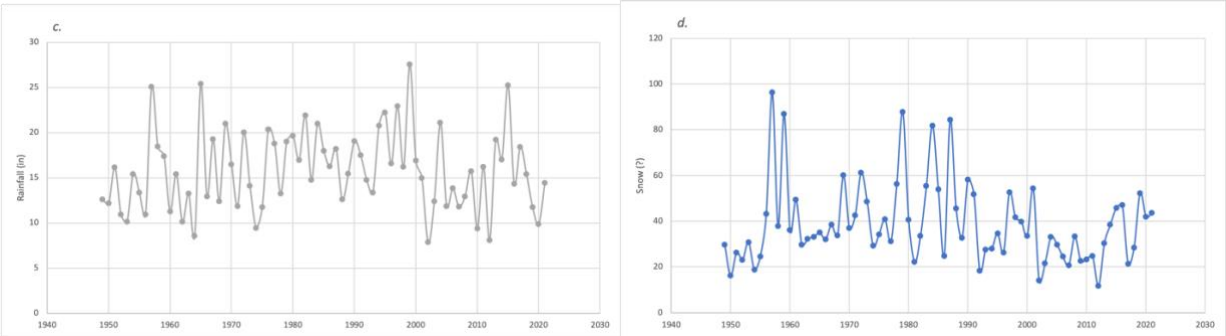

Figure 3. Climate data provided by Colorado Climate Center from 1949-2021. *a)* Maxima annual temperatures in C° *b)* minima annual temperatures in C° *c)* annual precipitation measured in inches *d)* annual snowfall. Each data contains annual averages from daily measurements.

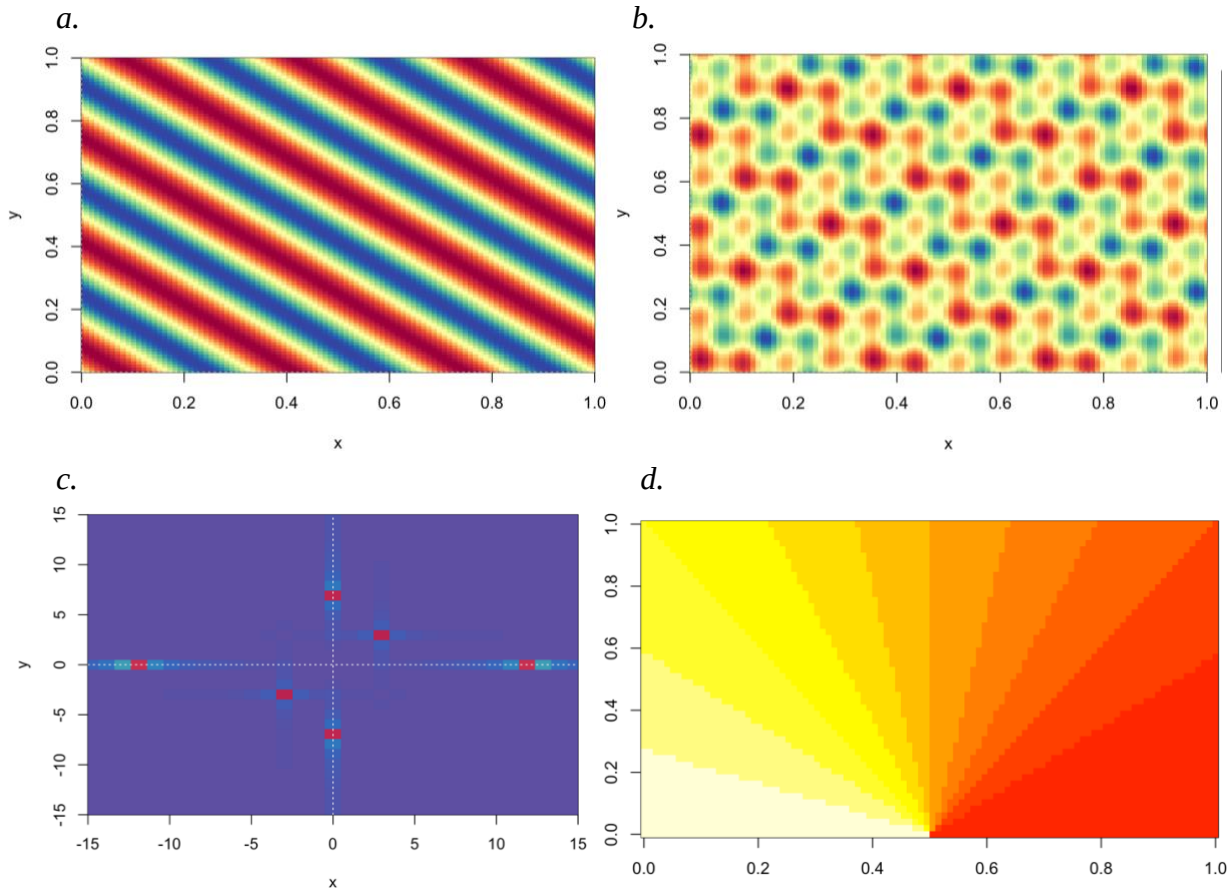

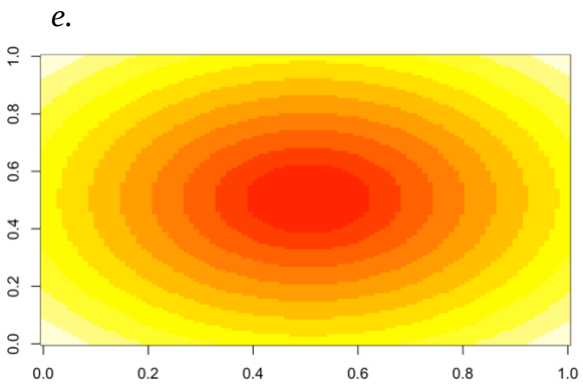

Figure 4. Simulated data from the theory R studio code. *a*) a simulated propagating N-S wave that repeats with a frequency of 3 and amplitude of 2; *b)* a simulated complex wave pattern that combines three propagating waves. One wave is the N-S wave from *a*) combined with E-W and diagonal waves; *c)* the periodogram for the complex wave pattern*; d)* the theta spectrum matrix*; e)* the radial spectrum matrix.

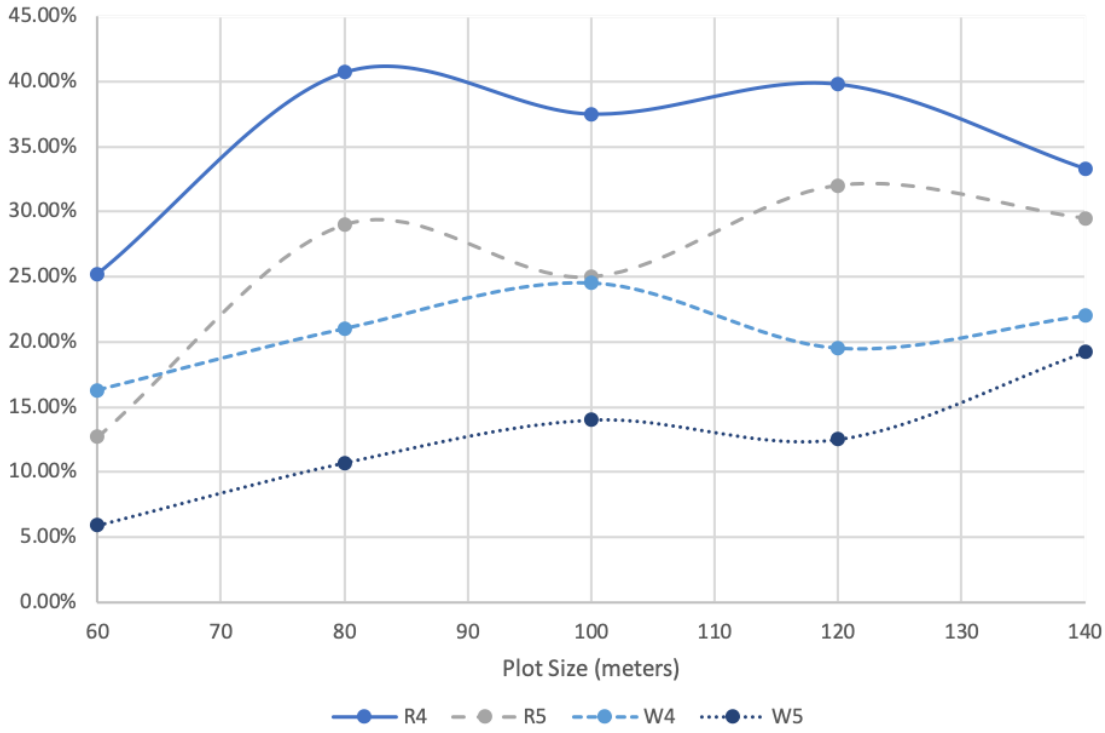

Figure 5. Exploration of using the wavelength of 4 or 5 as the statistically significant cutoff for banded vegetation patterns at Chico Basin Ranch. R4 and R5 are the overall percent of the AOI with significant banded vegetation patterns from the radial spectrum analysis, whereas W4 and W5 are the overall percent of dominant waves in the AOI.

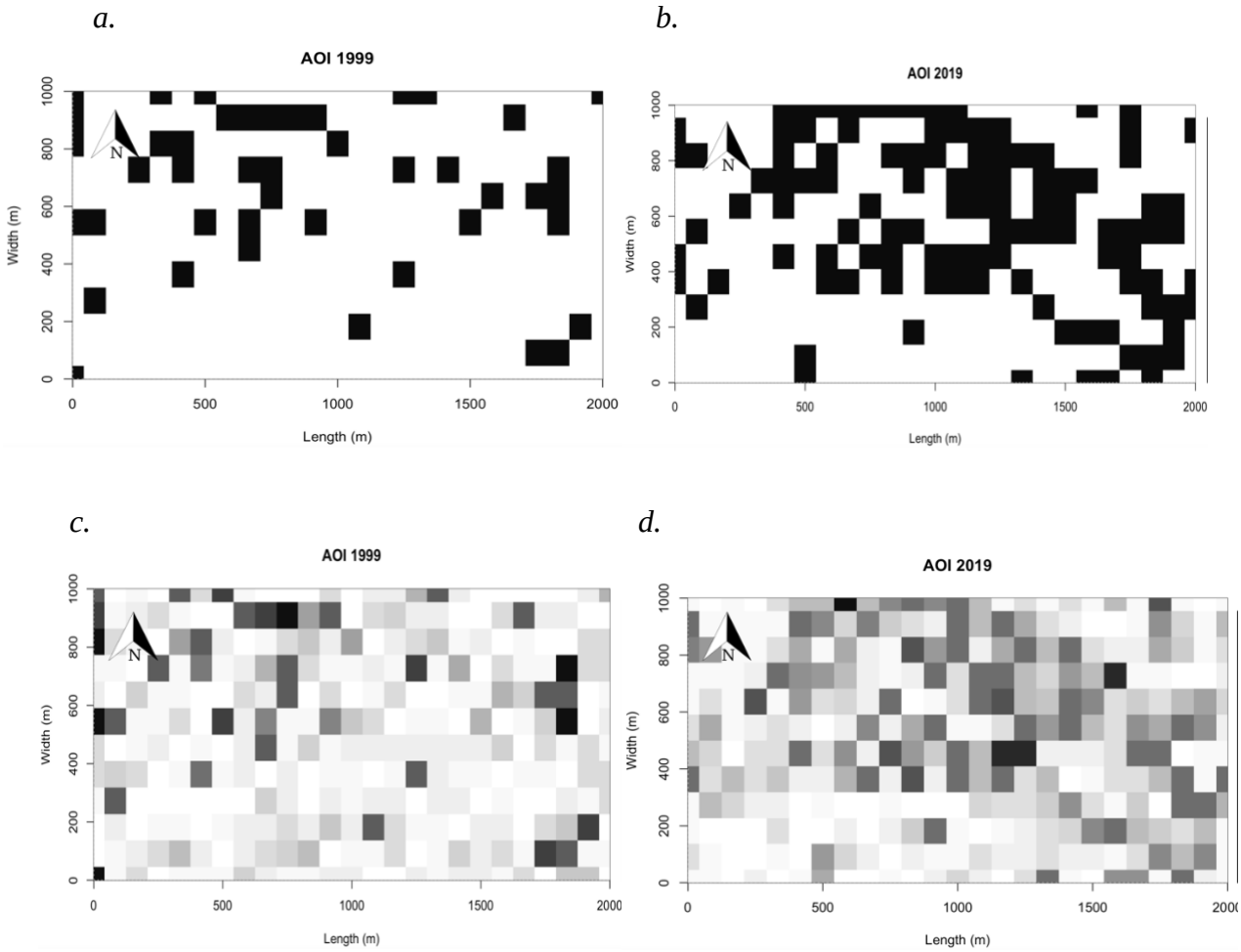

Figure 6. Maps of radial spectrum analysis results of the 1000x2000 m AOI in 1999 & 2019. *a)* and *b)* show the tiles in black with statistically significant banded vegetation patterns with a wavelength >4 in 1999 vs. 2019. *c)* and *d)* show the tiles at a gradient with vegetation patterning. The darkest tiles have the longest wavelengths. The white tiles have a dominant wavenumber of 1, which indicates that the dominant wave repeated itself once in the tile and hence the pattern is clearly aperiodic.

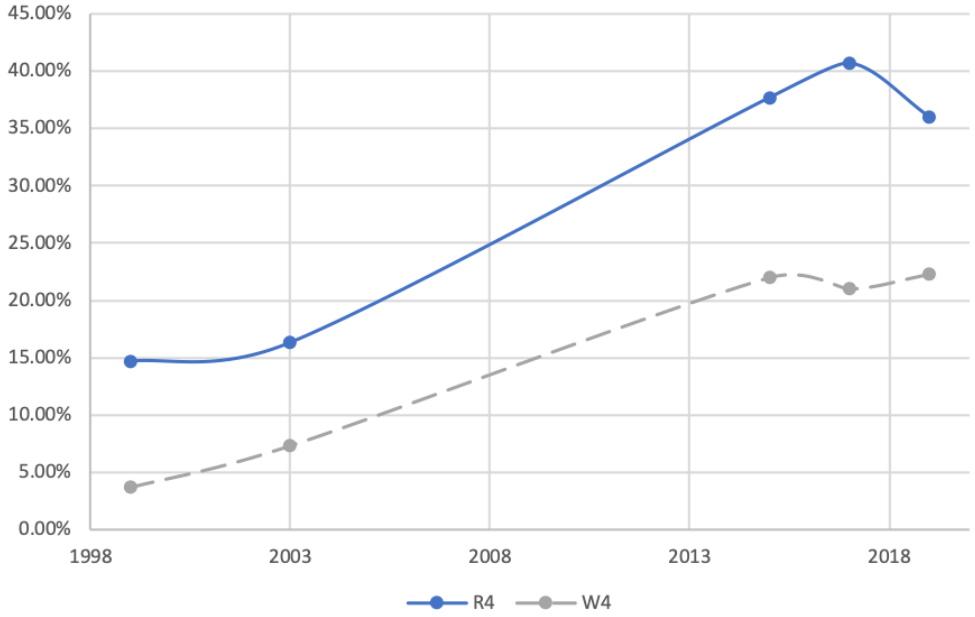

Figure 7. Percentage of statistically significant banded vegetation patterning (R4) and dominant wavelengths (W4) with a wavelength >4 in the AOI from 1999 to 2019.

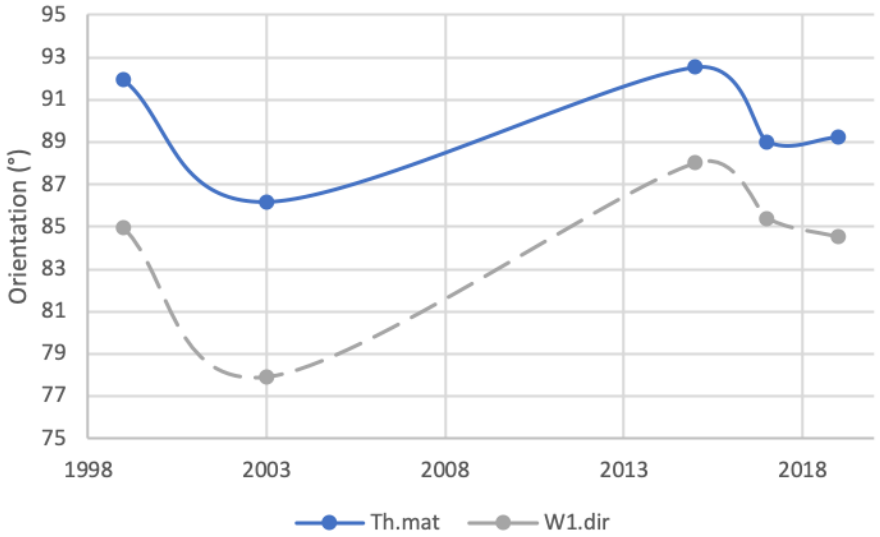

Figure 8. Orientation of the statistically significant banded vegetation patterns and dominant wavelengths from 1999 to 2019.

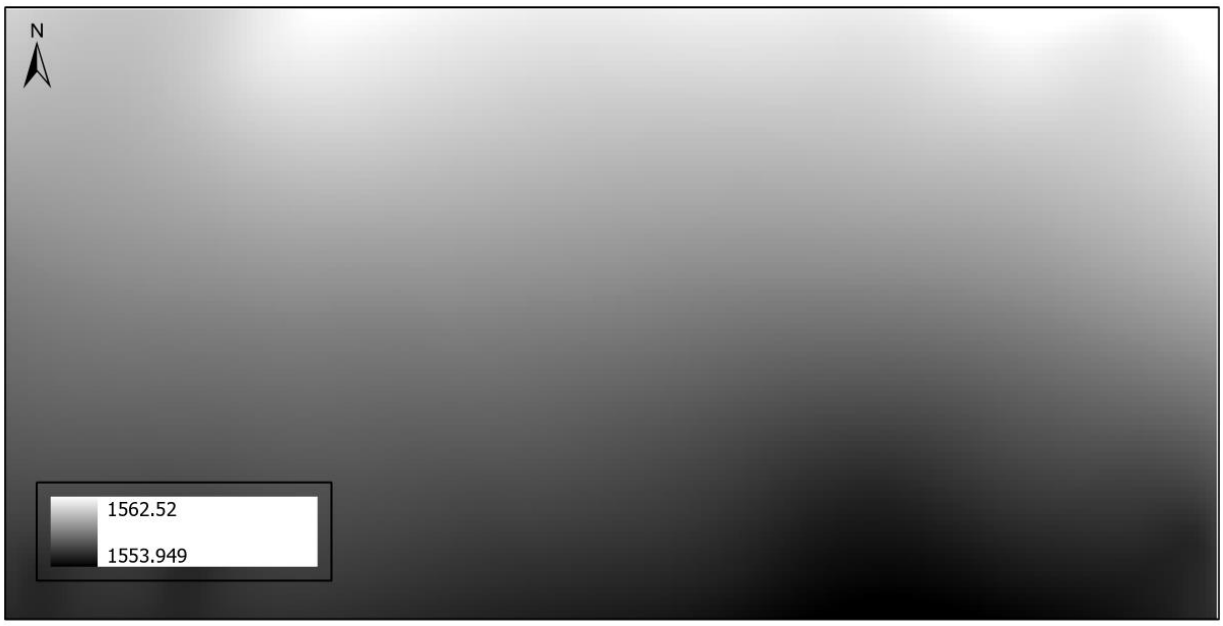

Figure 9. The slope orientation of the AOI shown in a white.- black gradient. White shows higher points which become darker as they slope downward.

Citations

Bokulich, A. (2014). How the Tiger Bush Got Its Stripes: "How Possibly" vs. "How Actually" Model Explanations. *The Monist*, *97*(3), 321–338. http://www.jstor.org/stable/44012688.

CHEN, Y., KOLOKOLNIKOV, T., TZOU, J., & GAI, C. (2015). Patterned vegetation, tipping points, and the rate of climate change. *European Journal of Applied Mathematics*, *26*(6), 945-958. doi:10.1017/S0956792515000261

Colorado Climate Center

Dunkerley, D. (2018). Banded vegetation in some Australian semi-arid landscapes: 20 years of field observations to support the development and evaluation of numerical models of vegetation pattern evolution. *Desert*, *23*(2), 165-187.

Dunkerley, D. (1999). Cellular automata: the exploration of spatial phenomena in ecology. pp.145- 183 in A.H. Fielding (Ed.) Machine learning methods for ecological applications, Boston: Kluwer Academic, 261pp.

Foster, E. (2021). Identifying Variations within the Runoff-Runon System of Self-Organizing Arid Vegetation.

Holmgren, M., and M. Scheffer. (2001). El Niño as a window of opportunity for the restoration of degraded arid ecosystems. Ecosystems 4:151–159.

Ludwig, J.A., Tongway, D.J., Marsden, S.G., 1998. Stripes, strands or stipples: Modelling the influences of three landscape banding patterns on resource capture and productivity in semi-arid woodlands, Australia. Catena, this issue.

Noy-Meir, I. (1973). Desert Ecosystems: environment and producers. Annu. Rev. Ecol. Systematics 4, 25-51.

Penny, G. G., Daniels, K. E., & Thompson, S. E. (2013). Local properties of patterned vegetation: quantifying endogenous and exogenous effects. *Philosophical Transactions of the Royal Society A: Mathematical, Physical and Engineering Sciences*, *371*(2004), 20120359.

Renshaw, E. and Ford, E.D. (1984). The Description of Spatial Pattern Using Two-Dimensional Spectral Analysis, *Vegetation*, 56:75-85.

Rietkerk, M., and van devKoppel, J. (1997). Alternate stable states and threshold effects in semi-arid grazing systems. Oikos, 69-76.

Rietkerk, M., MC. Boerlijst, F. van Langevelde, R. HilleRisLambers, J. van de Koppel, L. Kumar, HHT. Prins, AM. de Roos, 2002. Self-organization of vegetation in arid ecosystems. The American Naturalist, 160; 524-530.

Rietkerk, M., SC. Dekker, SC., de Ruiter, PC., van devKoppel, J. (2004). Self-organised patchiness and catastrophic shifts in ecosystems. Science, 305; 1926-1929. DOI: 10.1126/science.1101867.

Rondeau, R.J., G.A. Doyle, and K. Decker. 2016. Vegetation Monitoring at Pueblo Chemical Depot: 1999-2015. Colorado Natural Heritage Program, Colorado State University, Fort Collins, Colorado.

Scheffer, M., Carpenter, S., Foley, J. A., Folke, C., & Walker, B. (2001). Catastrophic shifts in ecosystems. Nature, 413(6856), 591-596.

Scheffer, M., & Carpenter, S. R. (2003). Catastrophic regime shifts in ecosystems: linking theory to observation. Trends in ecology & evolution, 18(12), 648-656.

Turing, A. M. (1990). The chemical basis of morphogenesis. Bulletin of mathematical biology, 52(1), 153-197.

Valentin, C., d'Herbès, J. M., and Poesen, J. (1999). Soil and water components of banded vegetation patterns. *Catena*, *37*(1-2), 1-24.

Vandervaere, J. P., Peugeot, C., Vauclin, M., Jaramillo, R. A., & Lebel, T. (1997). Estimating hydraulic conductivity of crusted soils using disc infiltrometers and minitensiometers. *Journal of Hydrology*, *188*, 203-223.

Vega, E., and Montana, C. (2011). Effects of overgrazing and rainfall variability on the dynamics of semiarid banded vegetation patterns: A simulation study with cellular automata. *Journal of arid environments*, *75*(1), 70-77.